

Sinusoidal buckling behaviour of surface casing with negative friction in thawing permafrost



Peixin Sun ^a, Tingting Luo ^a, Baosheng Wang ^c, Weihao Yang ^{a,b,*}

^a State Key Laboratory for Geomechanics and Deep Underground Engineering, China University of Mining and Technology, Xuzhou, Jiangsu, China

^b School of Mechanics and Civil Engineering, China University of Mining and Technology, Xuzhou, Jiangsu, China

^c Shanghai Construction Group Co., Ltd., Shanghai, China

ARTICLE INFO

Keywords:

Sinusoidal buckling
Surface casing
Negative friction
Permafrost
Rayleigh-ritz method

ABSTRACT

During the development of oil fields in permafrost regions, once the surface casing buckling occurs under the formation thawing and subsidence, it will cause great economic losses. In this paper, sinusoidal buckling of surface casing under negative friction is studied and preliminarily discussed. Based on the Winkler foundation theory and considering the different distribution forms of negative friction and soil resistance, the elastic stability model of casing is established. Combining dimensionless and Rayleigh-Ritz method, the critical slenderness ratio of sinusoidal buckling is obtained. The influence of boundary conditions, soil resistance and negative friction distribution on casing stability is quantitatively analysed on the basis of sufficient data calculation. It is found that the product of the critical slenderness ratio and the square root of the strain at the lower boundary is a fixed value which only depends on the boundary conditions and the value of soil resistance parameter, and the negative friction of different distribution forms can be superimposed according to the principle of 'inverse square' of the critical slenderness ratio. On this basis, the approximate calculation formula of the critical slenderness ratio is obtained by fitting, and the average error is less than 0.4%. The numerical example shows that the increase of soil resistance will weaken the influence of negative friction distribution on the critical slenderness ratio significantly. The ability to resist sinusoidal buckling can be improved by increasing the constraint of the lower casing section and increasing the casing thickness.

1. Introduction

A significant amount of oil and gas fields in the world are located in the Arctic Circle and covered with the permafrost of hundreds of meters deep, such as the Greater Kuparuk Area on the North Slope and the Mackenzie Delta, or Eastern Siberia in Russia (Smith, 1983; DeGeer and Cathro, 1992). As oil or gas production, heat is transferred to the frozen soil around the well, which will induce thawing of soil. Studies have shown that after 20 years of service, sizes of thaw zone can reach more than 10 m in radius (Xie, 2009). As the permafrost thaws, pore ice and segregated ice change into water and volume decreases. As the excess pore water pressure dissipates and the effective stress increases, soil is compacted. The above factors lead to obvious subsidence of soil (Goodman 1975, 1977) and negative skin friction along the surface casing, which is commonly found in pile foundation (Poulos and Davis, 1980; Gabr et al., 1994). So the surface casing is faced with the risk of

buckling just like many types of tubing or string. In the previous years, prediction of drill strings buckling load has been a great challenge to the drilling industry considering many factors such as boundary conditions, friction and tool joints (Hajianmaleki and Daily, 2014). At the same time, the research on casing buckling theory can also provide guidance for the progress of casing running technology (Li et al., 2018).

Lubinski (1950) introduced the theory of elastic stability into string buckling analysis and then (Lubinski and Althouse, 1962) studied the force and deformation of drilling string in vertical wellbores under different working conditions, laying a foundation for future research. As for inclined straight wellbores, Paslay and Bogy (1964) obtained the sinusoidal buckling critical load considering the axial force, axial moment and gravity by energy methods; Dawson et al., (1982) brought up the expression for critical force of sinusoidal buckling. Mitchell and Goodman, (1976) established a thawing-subsidence model to explain the concepts of alternating strain, and then (1986) analysed the helical

* Corresponding author. State Key Laboratory for Geomechanics and Deep Underground Engineering, China University of Mining and Technology, Xuzhou, Jiangsu, China.

E-mail address: sunpeixin@cumt.edu.cn (W. Yang).

buckling of tubing with friction. Wu (1992, Wu et al., 1993) conducted experimental studies on string buckling behavior in extended and horizontal wells and found that when helical buckling occurred, friction would increase sharply and even lead to self-locking. Gao and Miska (2009) derived a group of fourth-order nonlinear ordinary differential equations which were normalized to make the solutions independent of physical quantities. Their results show that the effect of the boundary conditions can be neglected when the dimensionless length of tubing is greater than 5π . Furthermore, the effects of friction on sinusoidal buckling were investigated using the principle of virtual work. Zhao and Gao (2011) described thermal buckling caused by thermal loading in a poor cement-bonding section or cement empty section. the arc length of sinusoidal and helical buckling is calculated. Morita and Shiozawa (2014) analysed the casing deformation data of Gulf of Mexico sandstone and North Sea Chalk, he believed that the casing damage there is related to the mechanical properties after the yield point and gave fitting curves of maximum stress and maximum strain of local buckling, both of which are proportional to thickness. Yue et al. (2017) derived the critical load of sinusoidal and helical buckling with the wellbore pressure at the bottom and the results are consistent with their experimental. Li and Samuel (2019) brought up a sinusoidal buckling model for the concentric strings in the transition mode which is derived based on the minimum energy theory. The new model was verified with Lubinski's literature and through a comparison with previous models, it is proved that the new model can make a better prediction of concentric strings buckling. Zhu et al. (2019 2020) set up a mechanical equilibrium equation for coiled tubing with an initial curvature in inclined wells and constant-curvature wellbores, based on the beam-column method. The model shows that compared with helical buckling, sinusoidal buckling is more easily influenced by initial curvature. Yang et al. (2020) used elastic-plastic finite element simulation to study the surface casing failure mechanism resulting from negative skin friction. The research results include ground subsidence; strain, stress and deformation of soil, casing-soil interface and casing; which can be well consistent with the field measured data. In addition, they discussed the applicability of the model and provided valuable experience for the study of casing stability.

In this paper, an idealized elastic model is proposed to analyse the interaction of underground structures using Rayleigh – Ritz method,

considering the soil resistance and negative friction around the surface casing. The potential energy equation of the casing - soil system is established. The slenderness ratio is used as the criterion of sinusoidal buckling, and the numerical solution of the critical slenderness ratio is obtained by programming using Matlab. Considering that numerical solutions are difficult to be extended and applied, this paper, on the basis of dimensionless variables, fits a large number of numerical solutions and obtains the formula for solving the critical slenderness ratio.

2. Formulation and solution

2.1. Models and assumptions

These basic assumptions need to be followed:

- (1) The axial shapes of casings and wellbores are completely consistent and casings direct contact with wellbores continuously and uniformly.
- (2) The casing string is considered as a linear elastic rod and its cross section always keeps annular.
- (3) Only the axial force and horizontal soil resistance are considered. Shear force is ignored.

Fig. 1 shows the schematic diagram of casing supporting conditions and forces. Considering the linear variation of negative friction along with the depth, we convert it to a linear load (taking the downward direction as the positive):

$$p = s + tX, \quad (0 \leq X \leq h) \quad (1)$$

Where, p is the linear load of the casing, N/m; s and t are coefficients representing negative friction, non-dimensional; X is vertical coordinate, m; h is the total length of the casing, m.

Theoretically, since s and t can be positive or negative, the negative friction distribution forms can be positive (or negative) rectangle, positive (or negative) triangle (or inverse triangle) and their combinations. Mitchell, (1986) concluded after a detailed study of oil well casing in Prudhoe Bay that the compressive strain at all depths was greater than

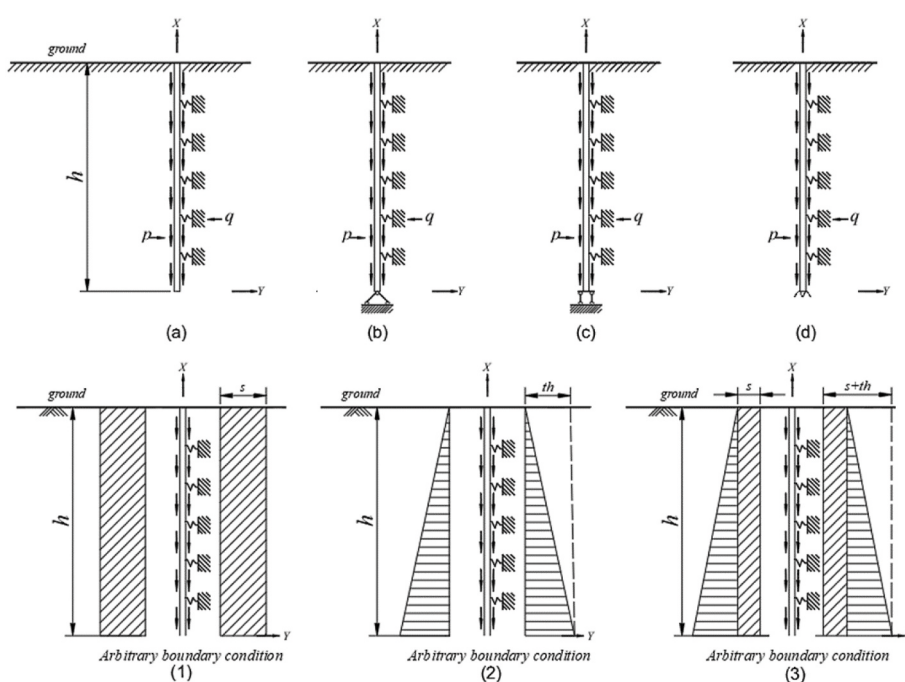


Fig. 1. Schematics of proposed model: (a) free end; (b) pinned end; (c) sliding end; (d) fixed end; (1) rectangular distribution; (2) triangular distribution; (3) trapezoid distribution.

the tensile strain, and the compressive strain increased uniformly with the thaw bulb radius. Therefore, the negative friction force is assumed to be distributed in triangular or trapezoidal shape. This hypothesis is also close to the researchers' judgment of geomechanics in Alaska (Yang et al., 2020). If $s = s_0$, $t = t_0 = -s_0/h$, then:

$$p = s_0 - (s_0/h)X, \quad (0 \leq X \leq h) \quad (2)$$

When $X = 0$, $p = s_0$; when $X = h$, $p = 0$. In this time, the negative friction distribution is triangle.

The horizontal resistance of the soil layer is assumed as Winkler foundation theory:

$$q = b_1 \psi Y \quad (3)$$

where q is horizontal resistance of the soil layer to the casing, N/m; b_1 is the calculated width of the casing, m; ψ is the coefficient of horizontal resistance of the soil layer, N/m³; Y is the deflection of the casing, m.

Based on the constant method or linear method, ψ can be respectively conformed to Eqs. (4) and (5):

$$\psi = \beta_0, \quad (0 \leq X \leq h) \quad (4)$$

$$\psi = \beta_1(h - X), \quad (0 \leq X \leq h) \quad (5)$$

where β_0, β_1 is the proportional coefficient of soil resistance coefficient, N/m³, N/m⁴. $\beta_0 \neq 0, \beta_1 = 0$ is the constant method while $\beta_0 = 0, \beta_1 \neq 0$ is the linear method.

2.2. Formula derivation and dimensionless

In order to determine the deflection of casing, it is necessary to analyse the deflection form of the casing. The uniform of deflection is

$$Y = C_{-1} + C_0 \frac{X}{h} + \sum_{n=1}^{\infty} C_n F_n \left(\frac{X}{h} \right) \quad (6)$$

where C_{-1}, C_0, C_n are undetermined coefficients, non-dimensional; $F_n \left(\frac{X}{h} \right)$ is linearly independent function that satisfies boundary conditions, non-dimensional.

The total potential energy of the system is the sum of bending strain energy of casing, elastic deformation energy of soil and load potential energy:

$$H = \frac{EI}{2} \int_0^h (Y'')^2 dX + \frac{1}{2} \int_0^{bh} qY dX - \int_0^{bh} p\omega(X) dX \quad (7)$$

where E is the elasticity modulus of casing, Pa; I is the inertia moment, m⁴; ω is the axial displacement of the casing, m.

$$\omega(X) = \frac{1}{2} \int_0^X (Y')^2 dX \quad (8)$$

Table 1
Trial-solution functions under different boundary conditions.

boundary conditions		$y = c_{-1} + c_0 x + \sum_{n=1}^{\infty} c_n f_n(x)$				checking	
top ($x = 1$)	Bottom ($x = 0$)	c_{-1}	c_0	$f_n(x)$	k	$x = 0$	$x = 1$
free	$y \neq 0$	free	$y \neq 0$	$\neq 0$	$\neq 0$	$\sin(kx)$	$y = c_{-1}$
	$y' \neq 0$		$y' \neq 0$				$y = c_{-1} + c_0$
	$y'' = 0$		$y'' = 0$			$y' = c_0 + \sum_{n=1}^{\infty} kc_n$	$y' = c_0 + \sum_{n=1}^{\infty} (-1)^n kc_n$
	pinned	$y = 0$	0	$\neq 0$	$\sin(kx)$	$y = 0$	$y = 0$
			$y' \neq 0$			$y' = c_0 + \sum_{n=1}^{\infty} kc_n$	$y' = c_0 + \sum_{n=1}^{\infty} (-1)^n kc_n$
	sliding	$y \neq 0$	$\neq 0$	0	$\cos(kx)$	$y = c_{-1} + \sum_{n=1}^{\infty} c_n$	$y = c_{-1}$
			$y' = 0$			$y' = 0$	$y' = \sum_{n=1}^{\infty} (-1)^n kc_n$
	fixed	$y = 0$	0	0	$1 - \cos(kx)$	$y = 0$	$y = \sum_{n=1}^{\infty} c_n$
			$y' = 0$			$y' = 0$	$y' = \sum_{n=1}^{\infty} (-1)^{n+1} kc_n$

Making $y = \frac{Y}{h}x = \frac{x}{h}, c_{-1} = \frac{C_{-1}}{h}, c_0 = \frac{C_0}{h}, c_n = \frac{C_n}{h}$, then Eq. (6) is nondimensionalized as

$$y = c_{-1} + c_0 x + \sum_{n=1}^{\infty} c_n f_n(x). \quad (9)$$

Eq. (9) can be further determined according to Table 1.

Eq. (7) can be nondimensionalized as:

$$\begin{aligned} \Omega &= \frac{h}{EI} \Pi = \frac{1}{2} \int_0^1 (y'')^2 dx + \frac{h^4 b_1}{2EI} \int_0^1 [\beta_0 + \beta_1 h(1-x)] y^2 dx \\ &\quad - \frac{h^3}{2EI} \int_0^1 p \left(\int_0^x (y')^2 dx \right) dx = \Omega_1 + \Omega_2 + \Omega_3 \end{aligned} \quad (10)$$

where Ω_1 represents bending strain energy of casing; Ω_2 represents elastic deformation energy of soil; Ω_3 represents potential energy which is consumed when friction works. All of them are non-dimensional.

Further, all variables in Ω_1, Ω_2 and Ω_3 can be nondimensionalized according to their physical significance:

$$\lambda = h \sqrt{\frac{A}{I}}, \epsilon_r = \frac{sh}{EA}, \epsilon_* = \frac{th^2}{2EA}, \epsilon_t = \frac{sh}{EA} + \frac{th^2}{2EA}, \zeta_1 = \sqrt[4]{\frac{\beta_0 b_1}{EI}} h, \zeta_2 = \sqrt[5]{\frac{\beta_1 b_1}{EI}} h \quad (11)$$

where λ is the slenderness ratio of casing, non-dimensional; A is the cross sectional area of casing, m²; I is the section moment of inertia, m⁴; E is the elastic modulus, N/m²; ϵ_r is the strain at the bottom of casing caused by rectangular negative friction; ϵ_* is the strain at the bottom of the casing caused by the distributive force of an inverted triangle. It is the compressive strain when $t > 0$ and the tensile strain when $t < 0$; ϵ_t is the strain at the bottom of the casing caused by distributional force of a combination of rectangle and inverted triangular friction. In the following text, for the sake of analysis, we will always take $t = -s/h$, so that ϵ_t represents the compressive strain due to the negative friction of the triangle distribution. ζ_1, ζ_2 is the represents soil resistance, non-dimensional.

According to the energy principle, the necessary and sufficient condition for the system to be in the critical equilibrium state is $\frac{\partial \Omega}{\partial c_i} = 0, i = -1, 0, 1, \dots, \infty$.

Taking the partial derivative of Ω_1 :

$$\frac{\partial \Omega_1}{\partial c_{-1}} = 0, \quad \frac{\partial \Omega_1}{\partial c_0} = 0, \quad \frac{\partial \Omega_1}{\partial c_i} = \sum_{n=1}^{\infty} T_{in} c_n, \quad i = 1, 2, \dots, \infty. \quad (12)$$

$$\text{where } T_{in} = \int_0^1 \int_n''(x) \int_i''(x) dx, \quad i = 1, 2, \dots, \infty.$$

Taking the partial derivative of Ω_2 :

$$\frac{\partial \Omega_2}{\partial c_{-1}} = J_{-1} c_{-1} + J_0 c_0 + \sum_{n=1}^{\infty} J_n c_n. \quad (13)$$

where $J_{-1} = \zeta_1^4 + \frac{1}{2}\zeta_1^5; J_0 = \frac{1}{2}\zeta_1^4 + \frac{1}{6}\zeta_1^5; J_n = \zeta_1^4 f_0 + \zeta_2^5 (f_0 - f_1); f_0 = \int_0^1 f_n(x) dx; f_1 = \int_0^1 f_n(x) x dx.$

$$\frac{\partial Q_2}{\partial c_0} = K_{-1}c_{-1} + K_0c_0 + \sum_{n=1}^{\infty} K_n c_n. \quad (14)$$

where $K_{-1} = J_0; K_0 = \frac{1}{3}\zeta_1^4 + \frac{1}{12}\zeta_1^5; K_n = \zeta_1^4 f_1 + \zeta_2^5 (f_1 - f_2); f_2 = \int_0^1 f_n(x) x^2 dx.$

$$\frac{\partial Q_2}{\partial c_0} = K_{-1}c_{-1} + K_0c_0 + \sum_{n=1}^{\infty} K_n c_n. \quad (15)$$

where $R_{in} = \zeta_1^4 R_{in0} + \zeta_2^5 (R_{in0} - R_{in1}); R_{in0} = \int_0^1 f_n(x) f_i(x) dx; R_{in1} = \int_0^1 f_n(x) f_i(x) x dx.$

Taking the partial derivative of Ω_3 :

$$\frac{\partial Q_1}{\partial c_{-1}} = 0, \quad \frac{\partial Q_3}{\partial c_0} = D_0 c_0 + \sum_{n=1}^{\infty} D_n c_n \quad (16)$$

where $D_0 = -\lambda^2 \left(\frac{\varepsilon_r}{2} + \frac{2\varepsilon_*}{3} \right); D_n = -\lambda^2 (\varepsilon_r g_0 + 2\varepsilon_* g_1); g_0 = \int_0^1 (\int_0^x f_n'(x) dx) dx; g_1 = \int_0^1 x (\int_0^x f_n'(x) dx) dx.$

$$\frac{\partial Q_3}{\partial c_i} = D_i c_0 + \sum_{n=1}^{\infty} F_{in} c_n, \quad i = 1, 2, \dots, \infty. \quad (17)$$

where $F_{in} = -\lambda^2 (\varepsilon_r F_{in0} + 2\varepsilon_* F_{in1}); F_{in0} = -\int_0^1 (\int_0^x f_n'(x) f_i'(x) dx) dx; F_{in1} = -\int_0^1 x (\int_0^x f_n'(x) f_i'(x) dx) dx.$

according to $\frac{\partial Q}{\partial c_{-1}} = \frac{\partial Q_1}{\partial c_{-1}} + \frac{\partial Q_2}{\partial c_{-1}} + \frac{\partial Q_3}{\partial c_{-1}} = 0;$

$$J_{-1}c_{-1} + J_0c_0 + \sum_{n=1}^{\infty} J_n c_n = 0. \quad (18)$$

according to $\frac{\partial Q}{\partial c_0} = \frac{\partial Q_1}{\partial c_0} + \frac{\partial Q_2}{\partial c_0} + \frac{\partial Q_3}{\partial c_0} = 0;$

$$K_{-1}c_{-1} + (K_0 + D_0)c_0 + \sum_{n=1}^{\infty} (K_n + D_n)c_n = 0. \quad (19)$$

according to $\frac{\partial Q}{\partial c_n} = \frac{\partial Q_1}{\partial c_n} + \frac{\partial Q_2}{\partial c_n} + \frac{\partial Q_3}{\partial c_n} = 0;$

$$J_i c_{-1} + (J_i + D_i)c_0 + \sum_{n=1}^{\infty} (R_{in} + T_{in} + F_{in})c_n = 0. \quad (20)$$

The necessary and sufficient condition for the nonzero solution of the linear homogeneous equations with undetermined coefficients is that the determinant of the coefficients is 0, that means:

$$|A| = \begin{vmatrix} J_{-1} & J_0 & J_1 & \cdots & J_n \\ J_0 & D_0 + K_0 & D_1 + K_1 & \cdots & D_n + K_n \\ J_1 & D_1 + K_1 & F_{11} + R_{11} + T_{11} & \cdots & F_{1n} + R_{1n} + T_{1n} \\ \vdots & \vdots & \vdots & \ddots & \vdots \\ J_i & D_i + K_i & F_{il} + R_{il} + T_{il} & \cdots & F_{in} + R_{in} + T_{in} \end{vmatrix} = 0 \quad (21)$$

For each group of $\varepsilon_r, \varepsilon_*, \zeta_1$ or ζ_2 , the critical slenderness ratio λ_{cr} can be determined by the calculation program.

2.3. Programming and solution

Based on dimensionless, the method of systematically solving λ_{cr} under different combination of working conditions is as follows: selecting a certain boundary condition and load combination, and

calculate the variables only related to them, including $T_{in}, f_0, f_1, f_2, R_{in0}, R_{in1}, D_0, D_n, g_0, g_1, F_{in}, F_{in0}, F_{in1}$. Then looping through different ζ and calculating the remaining variables including $J_{-1}, J_0, J_n, K_{-1}, K_0, K_n, R_{in}$. Finally, the variables are substituted into Eqn 21 to find the root by numerical method. Search method and dichotomy method are used in this paper. The calculation flow chart is shown in the appendix.

In the process of solving, it is necessary to correctly select the value of n , that is, the series of the flexure function 'Y'. The larger the value of n , the closer the deflection is to the real situation, therefore the calculated value of λ_{cr} gradually converges as the increase of n such as shown in Table 2. However, it can be seen from Eq. (21) that the number of determinant elements is $(n+1)^2$, and if n is too large, the efficiency of solution will be reduced significantly. Therefore, before the formal solution, we take the free top and fixed bottom as an example to study the convergence of the solution with n under different ζ . In Fig. 2, some integer values between 0 and 30 are taken for ζ_1 , which correspond to different color. The meaning of each line is that the value of λ_{cr} gradually converges as the order of the determinant n increases. n_c is defined as the n value when the degree of convergence is less than 0.1%, that is, the appropriate order of the determinant in the actual calculation. From the projection of $\zeta \sim n$ plane, it can be seen that n_c increases with the increase of ζ , and approximately satisfies:

$$n_c = \left[\frac{\zeta}{1.2} \right] + 2 \quad (22)$$

2.4. Verification of the solution

In order to verify the correctness of the formula derivation and calculation program in this section, the calculated results are compared with those of 'buckling of rod under distributed axial load' calculated by Timoshenko in his book *Theory of Elastic Stability*. When ζ_1 or ζ_2 approaches to zero, the deflection of the casing will not be constrained by lateral resistance, that is, it will degenerate into the buckling problem of the compressed rod as Timoshenko's research, and the critical load is expressed as: $P_{cr} = \frac{7.837EI}{h^2}$ (one end is free and another is fixed). It can be converted into the expression of the critical slenderness ratio: $\lambda_{cr} = \sqrt{\frac{7.837}{\varepsilon_r}}$. As shown in Table 3, the results of in this paper are entirely consistent with Timoshenko's when $\zeta = 0.1$, which proves that the formula deduced above is correct after degeneration and the solution below is credible.

3. Results and fitting

3.1. Relationship between λ_{cr} and ε

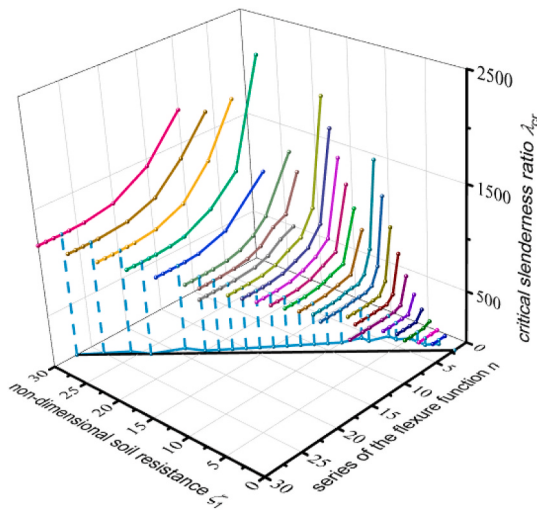
λ_{cr} is the function of the strain at the bottom of the casing ' ε (ε_r or ε_t)' and the non-dimensional soil resistance ' ζ (ζ_1 or ζ_2)'. Firstly, the relationship between λ_{cr} and ε need to be found under given ζ and boundary conditions. Fig. 3 (a)~(d) shows the scatter diagram and its fitting curve of λ_{cr} changing with ε under the boundary conditions of 'free-free', 'free-pinned', 'free-sliding', 'free-fixed' respectively. Fig. 3 not only includes different forms of negative friction distribution (rectangular or triangular), but also includes different forms of soil resistance change with depth (independent or linear increase). The fitting result shows that: square root of ε_r or ε_t is inversely proportional to λ_{cr} .

3.2. 'K' – the coefficient of stability

Because in this paper both ε_r and ε_t are compressive strain (greater

Table 2Calculated value of λ_{cr} and degree of convergence vs. the series of the flexure function 'n'.

Series of the flexure function (n)	$\zeta = 3$		$\zeta = 5$		$\zeta = 10$	
	calculated value	degree of convergence	calculated value	degree of convergence	calculated value	degree of convergence
1	187.8711	7.7380%	596.1914	71.3251%	3334.1796	262.7728%
2	183.7305	2.3969%	351.1133	0.8980%	1507.9495	64.0712%
4	179.7070	0.1672%	348.3398	0.1010%	975.2539	6.1117%
6	179.4727	0.0218%	348.0664	0.0224%	954.4727	3.8506%
8	179.4336	0.0000%	348.0273	0.0112%	920.4102	0.1445%
10	179.4336	0.0000%	347.9883	0.0000%	919.1992	0.0127%
12	179.4336	0.0000%	347.9883	0.0000%	919.0820	0.0000%
14	179.4336	0.0000%	347.9883	0.0000%	919.0820	0.0000%

**Fig. 2.** The convergence of the solution with n under different ζ

than zero), therefore the relationship of λ_{cr} and ε can be expressed as following:

$$\begin{aligned}\lambda_{cr} &= \frac{K_r}{\sqrt{\varepsilon_r}} \\ \lambda_{cr} &= \frac{K_t}{\sqrt{\varepsilon_t}}\end{aligned}\quad (23)$$

Where K_r and K_t are non-dimensional constant, which change with boundary conditions and ζ . The variation law of K_r and K_t calculated under different boundary conditions and method (constant or linear) has significant different as shown in Fig. 4 and Fig. 5.

In Fig. 4(a), when $\zeta > 4$, K_r of fixed bottom is about 2 times of free

bottom, 1.2 times of sliding bottom and pinned bottom. When ζ tends to zero, K_r of fixed bottom and sliding bottom tends to be the same value (about 2.80), however it tends to zero of pinned and free bottom. This indicates that limiting the bottom rotation angle can improve the casing stability better than limiting the bottom displacement, which is consistent with Euler's stability theory. The shape of curve in Fig. 4(b) is as same as that in Fig. 4(a), except the value is slightly higher. Obviously, the closer the load distribution of the same size is to the top, the more likely it is to cause instability.

In Fig. 5(a), when ζ tends to 0, K_r of different bottom supporting conditions is the same as which in Fig. 4(a). When $0 < \zeta \leq 2$, K_r of fixed and sliding bottom respectively increase from 2.80 to 3.41 and 3.15, which shows that the stiffness of thawed permafrost is small and the influence of soil resistance on casing stability is negligible. K_r of pinned and free bottom respectively increase from 0 to 2.30 and 1.33, which shows that soil resistance makes up for the deficiency of bottom constraints and improves the stability of casing. When $2 < \zeta \leq 4$, the stability of casing under different bottom boundary conditions is significantly improved. When $\zeta > 4$, K_r of four kinds of boundary conditions are approximate linear increase with ζ : fixed > sliding \approx pinned > free. Lee et al. (2018) used fourth-order Runge-Kutta method to solve the governing differential equation when studying the buckling of tapered friction piles. The curves of buckling load factor versus pile-soil stiffness is obtained whose shape is similar to Figs. 4 and 5.

When the boundary conditions and the distribution of load and soil resistance are determined, the K_r and K_t are functions of ζ . After comparison and selection, the fitting formulae were obtained by piecewise polynomial fitting method as shown in Eq. (24), because when $\zeta < 4$, the type of lines is obviously curved, and when $\zeta > 4$, it is approximately straight as shown in Eq. (24) and the parameters are shown in Tables 4 and 5. The comparison between the fitting curves and the original curves in Figs. 4 and 5 proves that the fitting effect is rational.

Table 3

A comparison of solution of this paper and Timoshenko.

λ_{cr}	free-fixed						Timoshenko solution					
	ζ_1						ζ_2					
	2.0	1.6	1.2	0.8	0.4	0.1	2.0	1.6	1.2	0.8	0.4	0.1
$\varepsilon_r = 0.001$	133.6	109.4	95.6	90.0	88.6	88.5	107.9	95.4	90.2	88.6	88.6	88.5
$\varepsilon_r = 0.005$	59.8	48.9	42.8	40.3	39.6	39.6	48.3	42.7	40.4	39.6	39.6	39.6
$\varepsilon_r = 0.01$	42.3	34.6	30.2	28.5	28.0	28.0	34.1	30.2	28.5	28.0	28.0	28.0

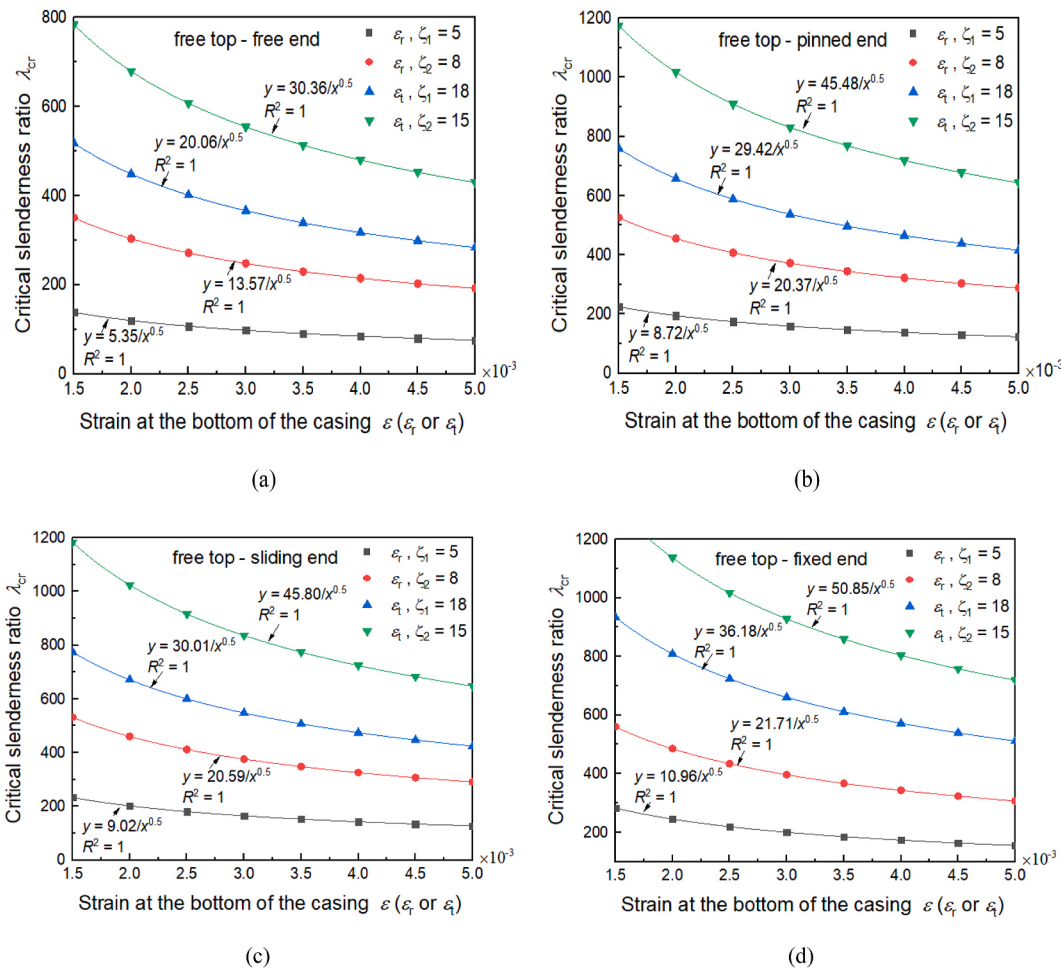


Fig. 3. λ_{cr} vs. ε : (a) free end; (b) pinned end; (c) sliding end; (d) fixed end.

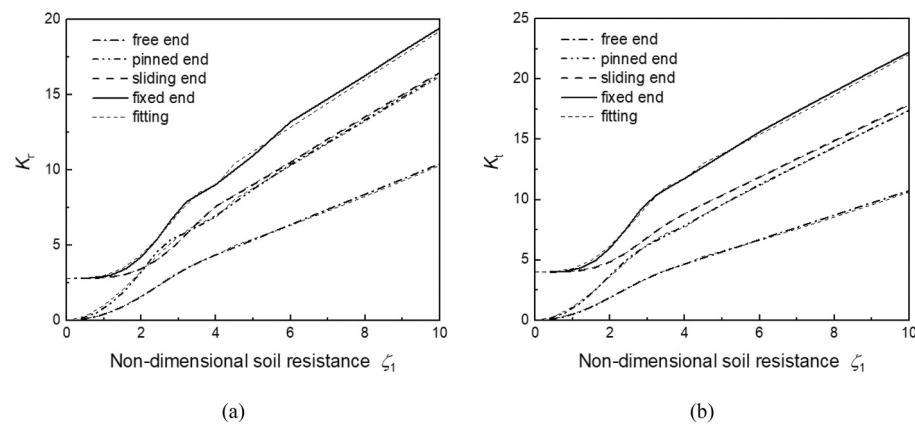


Fig. 4. Original and fitting curves of $K \sim \zeta_1$ under different boundary conditions used constant method: (a) K_r vs. ζ_1 ; (b) K_t vs. ζ_1 .

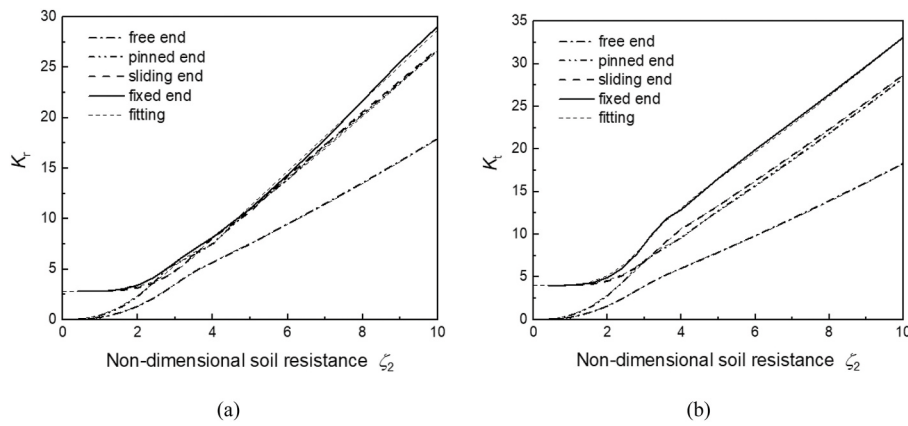


Fig. 5. Original and fitting curves of $K \sim \zeta_2$ under different boundary conditions used linear method: (a) K_r vs. ζ_2 ; (b) K_t vs. ζ_2 .

Table 4
Parameters of fitting formulae (constant method).

	rectangular distribution				triangular distribution			
	free end	pinned end	sliding end	fixed end	free end	pinned end	sliding end	fixed end
k_1	0.6011	1.198	0.0621	0.654	0.669	1.335	0.094	0.470
n_1	2.428	2.000	4.217	3.800	2.223	2.017	3.675	3.400
k_2	-0.2041	-0.1924	-0.016	-0.471	-0.155	-0.221	-0.010	-0.174
n_2	3.000	3.000	2.800	2.800	3.000	3.000	5.000	4.000
k_3	-	-	-	-	-	-	4.000	4.000
l_1	0.459	1.481	1.473	1.597	0.410	1.924	1.336	1.163
m	1.262	1.000	1.000	1.000	1.302	0.932	1.037	1.119
l_2	1.921	1.393	1.711	3.261	2.404	0.957	3.306	6.771

Table 5
Parameters of fitting formulae (linear method).

	rectangular distribution				triangular distribution			
	free end	pinned end	sliding end	fixed end	free end	pinned end	sliding end	fixed end
k_1	0.248	0.500	0.042	0.145	0.317	0.583	0.205	0.431
n_1	3.123	2.712	3.502	4.808	2.811	2.819	4.900	4.900
k_2	-0.051	-0.055	-	-0.106	-0.038	-0.076	-0.172	-0.367
n_2	4.000	4.000	-	5.000	4.000	4.000	5.000	5.000
k_3	-	-	2.800	2.800	-	-	4.000	4.000
l_1	0.837	2.021	2.001	3.076	0.819	1.764	1.585	2.103
m	1.315	1.152	1.154	1.042	1.323	1.195	1.226	1.155
l_2	0.620	-2.036	-1.763	-5.198	1.041	0.620	1.998	2.988

$$K = k_1 \zeta^{n_1} + k_2 \zeta^{n_2} + k_3, \quad (0 \leq \zeta < 4) \quad K = l_1 \zeta^m + l_2, \quad (4 \leq \zeta \leq 30) \quad (24)$$

Fig. 6 is the scatter plot of the increment of λ_{cr} under different non-dimensional soil resistance parameter ζ_1 and ζ_2 , when the distribution form of negative friction was changed from rectangular to triangular. The figures showed that when ζ was small ($\zeta_1 < 6$ or $\zeta_2 < 10$), the distribution form of negative friction had a significant effect on the critical slenderness ratio, especially for the case of 'free top and fixed end'. The difference of critical slenderness ratio reached 30% or 40% respectively ($\zeta_1 \rightarrow 0$ or $\zeta_2 = 4$).

3.3. Superposition principle

For a certain determined boundary condition and ζ , K_r or K_t , taking rectangle as an example, there is:

$$\varepsilon_r = \varepsilon_{r1} + \varepsilon_{r2} + \dots + \varepsilon_{rn} = \frac{K_r^2}{\lambda_{cr1}^2} + \frac{K_r^2}{\lambda_{cr2}^2} + \dots + \frac{K_r^2}{\lambda_{crn}^2} = \frac{K_r^2}{\lambda_{cr}^2} \quad (25)$$

K_r can be eliminated. That means if $\varepsilon_r = \varepsilon_{r1} + \varepsilon_{r2} + \dots + \varepsilon_{rn}$, there is:

$$\frac{1}{\lambda_{cr}^2} = \frac{1}{\lambda_{cr1}^2} + \frac{1}{\lambda_{cr2}^2} + \dots + \frac{1}{\lambda_{crn}^2} \quad (26)$$

This is the superposition principle of critical slenderness ratio under the same distribution of negative friction.

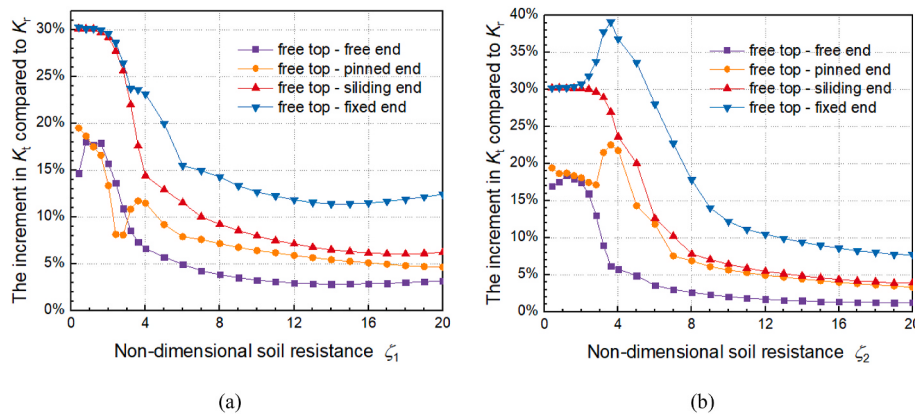


Fig. 6. The increment in K_t compared to K_r : (a) constant method; (b) linear method.

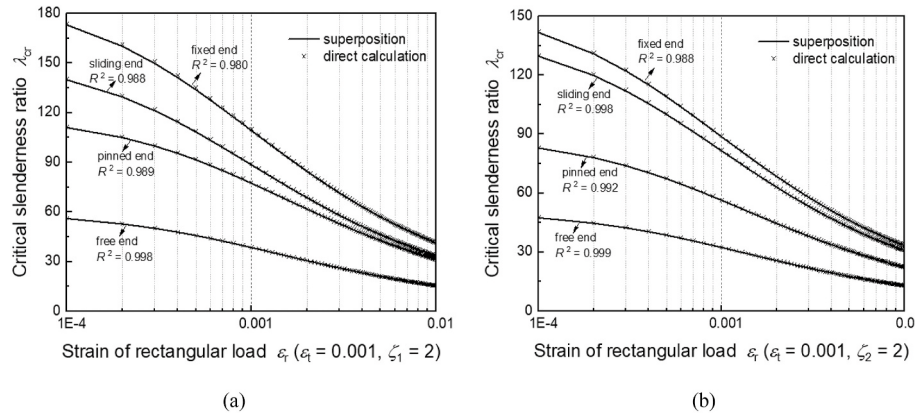


Fig. 7. Comparison of results obtained by superposition method and direct calculation: (a) constant method; (b) linear method.

In practical engineering, the radius of thaw bulb increases with depth and the distribution of negative friction is generally approximately trapezoid which corresponds to a set of specific values of s , t and h , as shown in Fig. 1(c). Calculations are needed to verify whether the critical slenderness ratio still satisfies the superposition principle under the action of negative friction with different distribution forms. The appropriate value of ζ needs to be selected to make a large difference between K_r and K_t . Because, as mentioned above, when K_r is equal to or approximately equal to K_t , the principle holds naturally. Only if the difference is obvious, can the superposition principle under different negative friction distributions be verified. According to Fig. 6, taking $\zeta = 2$, $\varepsilon_t = 0.001$, $\varepsilon_t = 0.0001\text{--}0.01$.

Fig. 7 is a comparison of the results calculated using the respective superposition method and the Rayleigh-Ritz method respectively. According to the statistics, the determination coefficients (R^2) of the real solutions fitted by superposition principle are all greater than 0.98, while the maximum error is less than 1.0% and the average error is less

than 0.4%. Therefore, there is sufficient reason to believe that the following formula is true:

$$\frac{1}{\lambda_{cr}^2} = \frac{1}{\lambda_{crr}^2} + \frac{1}{\lambda_{ctr}^2} \quad (27)$$

Substituting in Eq. (23), we get

$$\lambda_{cr} = \frac{K_t K_r}{\sqrt{\varepsilon_t K_t^2 + \varepsilon_r K_r^2}} \quad (28)$$

4. Example and discussion

Suppose an oil well on the permafrost area is going through permafrost at a depth of H and the J55-grade casing is used with the following material properties: elastic modulus $E = 2.1 \times 10^5$ MPa, yield strength $\sigma_y = 552$ MPa and the maximum elastic strain is 0.26%. The thickness of casing ' t_c ' have four options: 6.71 mm, 8.94 mm, 10.16 mm, 11.42 mm. The section area 'A' and section moment of inertia 'T' is shown in Table 6.

Considering the top of casing often appear obvious subsidence and the ground can't completely restrain its rotation angle, it is relatively safe to assume that the top of casing is unconstrained (free). If the bottom of casing is embedded in the rock, the boundary condition should be fixed. However, considering that elastic instability generally occurs only in the middle or upper part of casing, if only this part is taken as the research object, then the fixed constraint should be relaxed into sliding

Table 6
Section area and moment of inertia.

t_c/mm	6.71	8.94	10.16	11.42
$A/10^{-3} \times \text{m}^2$	4.4	5.9	6.7	7.4
$I/10^{-5} \times \text{m}^4$	2.5	3.3	3.7	4.0

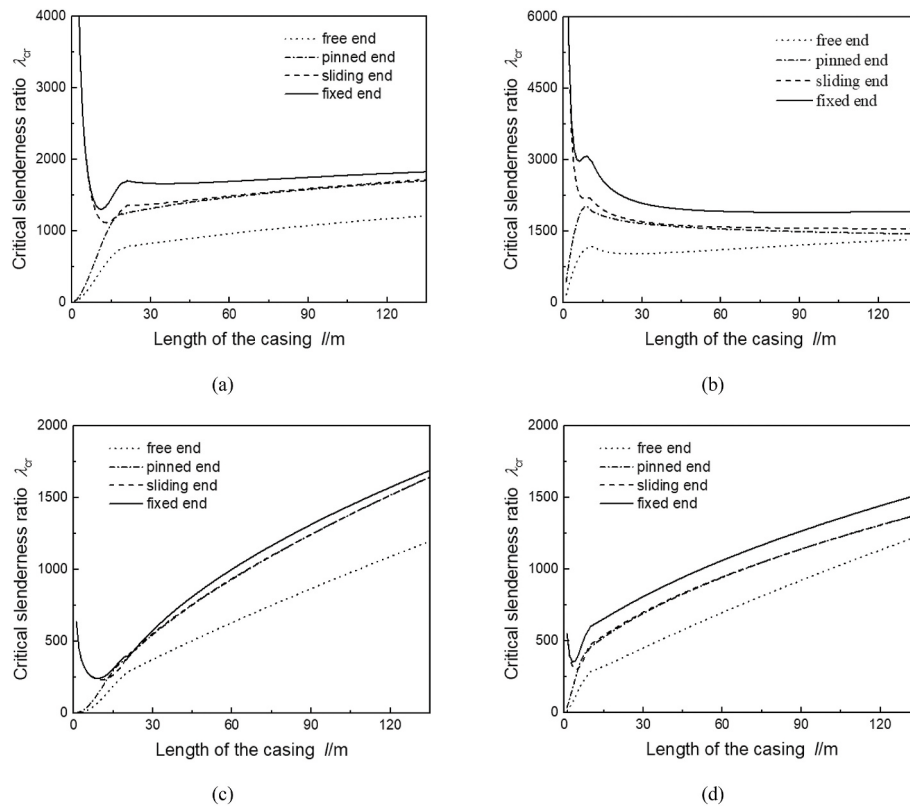


Fig. 8. Typical curves of λ_{cr} vs. l ($t_c = 11.42$ mm, $\beta_0 = 5h_{\max}\text{kN/m}^3$ or $\beta_1 = 10 \text{ kN/m}^4$): (a) $\varepsilon = \varepsilon_t$, linear method; (b) $\varepsilon = \varepsilon_t$, constant method; (c) $\varepsilon = \varepsilon_r$, linear method; (d) $\varepsilon = \varepsilon_r$, constant method.

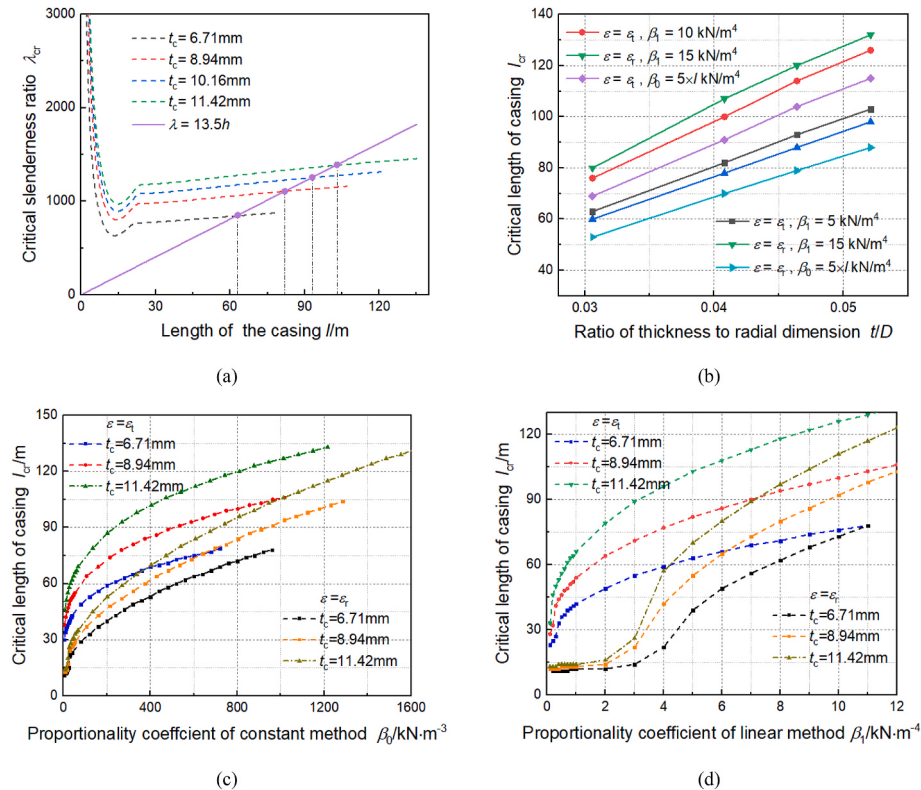


Fig. 9. Critical depth curves and the factors: (a) Determination of critical depth; (b) influence of thickness; (c) influence of β_0 ; (d) influence of β_1 .

constraint. In this example, two distribution of negative friction are considered: rectangular and triangular. In order to make the negative friction of different distribution forms equal, it should be satisfied: $t = 2 s/l$. Therefore, in this case, when the distribution is rectangular, there is $s = 3 \times 10^4 \text{ N/m}$, $t = 0$; when the distribution is triangular, there is $s = 0$, $t = (6 \times 10^4 \text{ N/m})/l$. According to (11), it can be calculated that when the length of casing is l , there is $\lambda \approx 13.5l$. When $l \leq l_{\max} = \frac{EA}{s}\epsilon_{\max}$, casing is in elastic state. Experts generally show that the bulb radius is smaller at the top and larger at the bottom, and the vertical section of bulb is approximately triangle or trapezoid. Therefore, the resistance distribution of permafrost soil in the oil field is much more complicated than that of unfrozen engineering. Due to the effect of ground stress, the deep soil should have a higher soil resistance coefficient, but the expansion of the thawing range of frozen soil will reduce the soil resistance to some extent. This is also the reason why constant and linear method are both considered in this paper. According to (3), (4) and (5), the soil resistance value is related to b_1 , $\beta_0(\beta_1)$ and l . Where b_1 is the constant in this example, and l is inversely proportional to s . That is when $\beta_0 = 0.5\beta_1 l$, the soil resistance obtained by constant method or linear method is equal. Therefore, in this example, when assuming that the horizontal resistance coefficient of the soil layer increases linearly with depth, there is $\beta_1 = 5, 10, 15 \text{ kN/m}^4$, $\beta_0 = 0$; when assuming that it is constant, there is $\beta_1 = 0$, $\beta_0 = 2.5l_{\max}$ or $5l_{\max}$ or $7.5l_{\max} \text{ kN/m}^3$. In the future research, they can be combined to match the distribution of real soil resistance better.

4.1. Typical curves of λ_{cr}

Each combination of negative friction, soil resistance coefficient and boundary conditions correspond to a unique shape of critical slenderness curves. Analysing the variation trend of critical slenderness ratio under different working conditions is helpful to deepen the understanding of elastic stability of surface casing. In Fig. 7, when $l \rightarrow 0$, for the case of sliding and fixed at the bottom, the λ_{cr} of triangular friction is higher than that of rectangular friction, which is due to significant differences in the magnitude of the load. For free and pinned ends, λ_{cr} tends to zero regardless of the distribution of negative friction. What is worth special attention here is that when $l > 15\text{m}$, the critical slenderness ratio corresponding to sliding end and pinned end is almost the same, however when $l < 15\text{m}$ ((d) is $l < 5\text{m}$), the difference between them gradually increases. This shows once again that when the casing or elastic bar is subjected to small external load or lateral constraint, the constraint of rotation angle can improve its stability better than the constraint of displacement. As the depth increases, it can be seen that the difference between sliding and pinned is weakened, and the two curves almost coincide.

In Fig. 8, with the exception of (b), there are obvious minimum points for the critical slenderness ratios in both fixed end and sliding end. This is because before the minimum point, the weakening effect of negative friction on stability is dominant. With the increase of depth, soil resistance constraint plays a dominant role in improving stability after the minimum point. For Fig. 8(b), the soil resistance coefficient is constant, while the negative friction increases linearly with depth, so there is no obvious growth stage of λ_{cr} . In practical petroleum engineering in cold regions, the formation which casing passes through is complex, and the distribution of negative friction and resistance coefficient may be very irregular. If hundreds of meters of casing can be separated into several segmentation, so that the distribution of external load in each one is more uniform, then the stability of casing can be checked in parts.

4.2. Effect of casing thickness ' t_c ', on l_{cr}

The intersection point in Fig. 9(a) indicates that when $\lambda = \lambda_{cr}$, the casing is in a critical state of elastic instability. The corresponding depth of thawing permafrost is defined as the critical length of the casing (l_{cr}). If the actual embedding depth of casing is greater than the critical embedding depth, there is a risk of elastic instability. Obviously, the thickness of casing and the stiffness of the surrounding soil will affect the critical embedding depth.

4.3. Effect of soil lateral resistance ' β_0 ', ' β_1 ' on l_{cr}

Fig. 9(b) shows that under any combination of negative friction distribution and soil resistance coefficient distribution, the critical length l_{cr} increases linearly with the ratio of thickness to radial dimension t/D , and the slope of the line is similar under different conditions. When t/D increases from 0.0306 to 0.0521, the critical length increases by 60%. This indicates that increasing the thickness of casing can effectively improve the buckling resistance of casing, and the influence of ' t/D ' on casing elastic stability is almost not affected by distribution of soil resistance or load.

Fig. 9(c) and (d) show the curve of l_{cr} and proportional coefficient β of soil resistance coefficient obtained by constant method and linear method respectively which consists of nonlinear segment and linear segment, and the slope decreases firstly and then remains unchanged as β increases (or increases firstly and then decreases and finally remains unchanged). Since β and load have been converted as described above to ensure the equality of 'values', the influence of different soil resistance distribution forms on l_{cr} can be reflected better by the trend of curves. Because the rectangular negative friction is closer to the upper end of the casing than the triangular negative friction, the critical length is smaller. The difference of critical length decreases as β_1 increases when using linear method. Even the effect of load distribution on the critical length can be eliminated if β_1 is large enough. However, when constant method is used, the influence of load distribution is always obvious. Analysing the effect of β on l_{cr} is helpful to select more appropriate parameters for complex models in solving practical engineering problems. For example, if the proportional coefficient distribution is difficult to be measured by experiment in the site, then parameters should be selected safer: it can be assumed that the negative friction force is distributed in rectangular or trapezoidal, and the linear method can be used to solve the critical slenderness ratio.

4.4. The limitations and prospects

- At present, this study only focuses on the elastic buckling of casing, and does not involve the plastic buckling. In the future research, plastic theory should be introduced to further improve the derivation of the formula.
- In order to facilitate the preliminary development of the work and search for the general law, the model in this paper is more ideal, and lacks the consideration of the influence of cement ring on sinusoidal buckling. However, cementing is an essential part of drilling operations, so it is necessary to discuss the impact of the cement ring here. First, the presence of the cement ring increases the contact area and friction coefficient between the casing and the wellbore, which increases the negative friction resistance, which is bad. However, the cement ring also increases the cross-sectional area and helps assume some of the vertical stress, thus reducing the drag load on the casing. In addition, the cement ring restrains the casing flexural deformation

- to some extent, which helps to improve the critical slenderness ratio. More importantly, the cement ring acts as an insulating layer between the casing and the permafrost, slowing the expansion of the thaw bulb. In the future, these effects of cement ring will be quantified as far as possible in order to gradually improve the sinusoidal buckling study of casing in thawing permafrost region.
3. Although four kinds of boundary conditions, two kinds of soil resistance distributions and two kinds of negative friction distributions (and their superpositions) are considered in this study, there are still some differences from the real site conditions. In the next step of the study, it is possible to consider splitting the casing into sections, each with its own unique load and resistance distribution, to better simulate the real situation.

5. Conclusions

In this study, a model for analysing the elastic stability of surface casing in permafrost area is presented. The dimensionless potential energy equation of the casing - thawing frozen soil system is established and the Rayleigh-Ritz method is used to solve the equation under different boundary conditions.

Through the analysis and discussion of a large number of numerical solutions, the following conclusions can be drawn:

- 1) Square root of ε_r or ε_t is inversely proportional to λ_{cr} . Inverse proportionality coefficient K is a non-dimensional parameter, which is related to boundary conditions, soil resistance, and distribution of load. The distribution of negative friction has a significant effect on the critical slenderness ratio. However, with the increase of soil resistance, the difference between rectangular distribution and triangular distribution gradually decreases from 40% to less than 10%. The negative frictional force acting on the whole length of casing satisfies the superposition principle even if the distribution forms are different : $\frac{1}{\lambda_{cr}^2} = \frac{1}{\lambda_{crr}^2} + \frac{1}{\lambda_{ctr}^2}$.

Nomenclature

A	Cross section area of casing, m^2
b_1	Calculated width of casing, m
C_1, C_0 and C_n	Undetermined coefficient, dimensionless
E	Young's modulus, N/m^2
h	Total length of casing, m
I	Section moment of inertia, m^4
K_r and K_t	Coefficient of stability, dimensionless
l	Length of casing (using in Section 4), m
l_{cr}	Critical length of casing, m
n	Series of the flexure function
p	Linear load of casing, N/m
P_{cr}	Critical load, N
q	Horizontal resistance of soil layer to the casing, N/m
s and t	Parameters to represent negative friction, dimensionless
X	Vertical coordinate, m
Y	Horizontal coordinate or deflection of casing, m
β_0 and β_1	Proportional coefficient of soil resistance coefficient, N/m^3 and N/m^4
ε_r and ε_t	Strain caused by rectangular and triangular negative friction, dimensionless
ζ_1 and ζ_2	Parameters to represent soil resistance, dimensionless
λ	Slenderness ratio, dimensionless
λ_{cr}	Critical slenderness ratio, dimensionless
ψ	Horizontal resistance of soil layer, N/m^3

- 2) In this paper, the calculational formula of the critical slenderness ratio is obtained by fitting. In engineering design, the parameter table (Table 2) can be consulted and substituted into this formula to conveniently calculate the critical slenderness ratio. In addition, when the distribution of the proportional coefficient of soil resistance is difficult to determine, it is suggested to use the linear method, and the distribution of negative friction should be rectangular or trapezoidal.
- 3) This paper suggests that in future studies, the appropriate series n of flexure function can be selected according to: $n_c = \left[\frac{\zeta}{1.2} \right] + 2$. In addition, future studies can also verify whether the formula satisfies other distribution of load or boundary and conditions.

Credit author statement

Peixin Sun: Methodology, Software, Formal analysis, Writing – Original Draft, Writing – Review & Editing. Weihao Yang: Conceptualization, Validation, Resources, Supervision, Funding acquisition. Tingting Luo: Resources, Writing – Review & Editing, Funding acquisition. Baosheng Wang: Formal analysis.

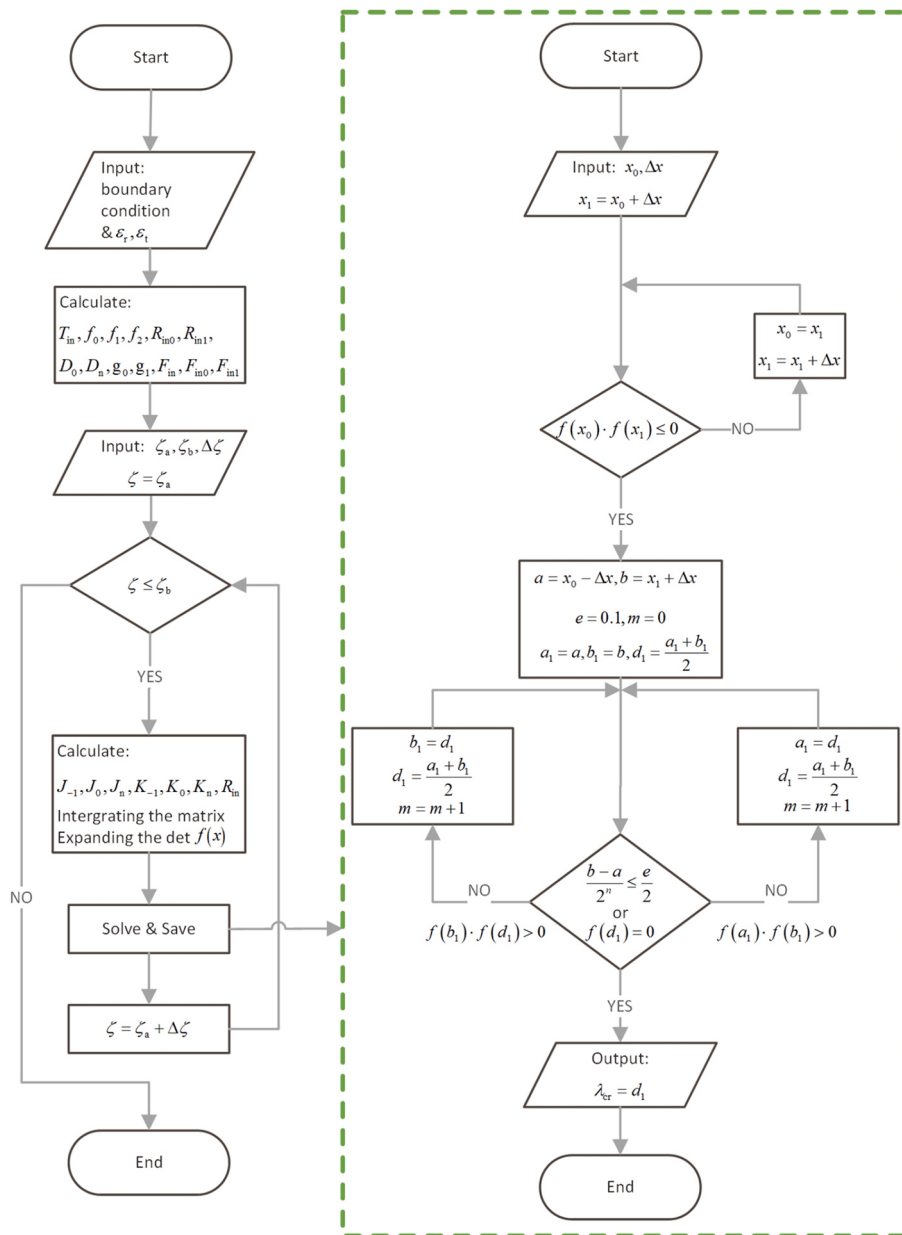
Declaration of competing interest

The authors declare that they have no known competing financial interests or personal relationships that could have appeared to influence the work reported in this paper.

Acknowledgements

This work was supported by funding from the National Key Research and Development Program of China (Grant No. 2016YFC0600904), the Natural Science Foundation of Jiangsu Province (Grant Nos. BK 20200653), and the Project funded by China postdoctoral Science Foundation (Grant No.2020M681768).

Appendix. Algorithm flow chart



References

- Dawson, R., Paslay, P.R., 1982. Drill Pipe Buckling in Inclined Holes. <https://doi.org/10.2118/11167-PA>. N.p., United States. Web.
- DeGeer, D.D., Cathro, D.C., 1992. Technology for Detecting Permafrost and Assessing its Impact on Hydrocarbon Production. C-FER and EBA Engineering Consultants Ltd, Edmonton, Alberta. C-FER Rep. 91-23.
- Gabr, M.A., Wang, J., Kiger, S.A., 1994. Effect of boundary conditions on buckling of friction piles. *J. Eng. Mech.* 120 (6), 1392–1400. [https://doi.org/10.1061/\(ASCE\)0733-9399\(1994\)120:6\(1392\)](https://doi.org/10.1061/(ASCE)0733-9399(1994)120:6(1392)).
- Gao, G., Miska, S.Z., 2009. Effects of boundary conditions and friction on static buckling of pipe in a horizontal well. *SPE J.* 14 (4), 782–796. <https://doi.org/10.2118/111511-PA>.
- Goodman, M.A., 1975. Mechanical properties of simulated deep permafrost. *J. Eng. Ind. Trans. ASME* 417–425. <https://doi.org/10.1115/1.3438601>.
- Goodman, M.A., 1977. Loading mechanisms in thawed permafrost around Arctic wells. *ASME J. Press. Vessel. Technol.* 99 (4), 641–645. <https://doi.org/10.1115/1.3454587>.
- Hajianmaleki, M., Daily, J.S., 2014. Advances in critical buckling load assessment for tubulars inside wellbores. *J. Pet. Sci. Eng.* 116, 136–144. <https://doi.org/10.1016/j.petrol.2014.02.019>.
- Lee, J.K., Jeong, S., Kim, Y., 2018. Buckling of tapered friction piles in inhomogeneous soil. *Comput. Geotech.* 97, 1–6. <https://doi.org/10.1016/j.compgeo.2017.12.012>.
- Li, C., Samuel, R., 2019. An improved model for concentric string buckling. *J. Pet. Sci. Eng.* 187, 106708. <https://doi.org/10.1016/j.petrol.2019.106708>.
- Li, W., Huang, G., Jing, Y., 2018. Modeling and mechanism analyzing of casing running with pick-up and release technique. *J. Pet. Sci. Eng.* 172, 538–546. <https://doi.org/10.1016/j.petrol.2018.09.099>.
- Lubinski, A., 1950. January. A study of the buckling of rotary drilling strings. In: *Drilling and Production Practice*. American Petroleum Institute.
- Lubinski, A., Althouse, W.S., 1962. Helical buckling of tubing sealed in packers. *J. Pet. Technol.* 14 (6), 655–670.
- Mitchell, R.F., Goodman, M.A., 1976. Permafrost thaw-subsidence casing design. *J. Pet. Technol.* 30 (3), 455–460. <https://doi.org/10.2118/6060-pa>.
- Mitchell, R.F., 1986. Simple frictional analysis of helical buckling of tubing. *SPE Drill. Eng.* 1 (6), 457–465. <https://doi.org/10.2118/13064-pa>.

- Morita, N., Shiozawa, S., 2014. Stability analysis of casings during plastic Deformation. In: Proc., SPE Deepwater Drilling and Completion Conf. Society of Petroleum Engineers, Richardson, TX, pp. 129–142. <https://doi.org/10.2118/170303-ms>.
- Paslay, P.R., Bogy, D.B., 1964. The stability of a circular rod laterally constrained to Be in contact with an inclined circular cylinder. *J. Appl. Mech.* 31 (4), 605–610. <https://doi.org/10.1115/1.3629721>.
- Poulos, H.G., Davis, E.H., 1980. *Pile Foundation Analysis and Design*, pp. 323–335.
- Smith, R.E., 1983. Development of petroleum reserves in Arctic Alaska: a brief discussion. *Cold Reg. Sci. Technol.* 7, 195–199. [https://doi.org/10.1016/0165-232X\(83\)90066-6](https://doi.org/10.1016/0165-232X(83)90066-6).
- Wu, J., 1992. *Buckling Behavior of Pipes in Directional and Horizontal Wells*. Texas A & M University, Texas.
- Wu, J., Juvkam-Wold, H.C., Lu, R., 1993. Helical buckling of pipes in extended reach and horizontal wells—Part 2: frictional drag analysis. *J. Energy Resour. Technol.* 115 (3), 196. <https://doi.org/10.1115/1.2905993>.
- Xie, J., 2009. Analysis of thaw subsidence impacts on production wells. In: Proc., SIMULIA Customer Conf. Dassault Systemes, London, pp. 1–14. Providence, RI. <https://www.researchgate.net/publication/308709687>.
- Yang, Z., Sun, T., Wang, J., Zhang, F., Zubeck, H., Aleshire, L., 2020. Well casing subsidence in thawing permafrost: a case study. *J. Cold Reg. Eng.* 34 (2) [https://doi.org/10.1061/\(asce\)cr.1943-5495.0000213](https://doi.org/10.1061/(asce)cr.1943-5495.0000213).
- Yue, Q., Liu, J., Dong, R., 2017. The research of post-buckling about slender rod string in wellbore based on energy method and experiment. *J. Pet. Sci. Eng.* 156 <https://doi.org/10.1016/j.petrol.2017.06.046>.
- Zhao, Z., Gao, D., 2011. Thermal buckling of casing in a slanted thermal production well. *Pet. Sci. Technol.* 29 (8), 769–803. <https://doi.org/10.1080/10916460903485827>.
- Zhu, Z., Zheng, L., Yang, H., 2019. Buckling behavior and axial load transfer assessment of coiled tubing with initial curvature in an inclined well. *J. Pet. Sci. Eng.* 173, 136–145. <https://doi.org/10.1016/j.petrol.2018.10.021>.
- Zhu, Z., Hu, G., Fu, B., 2020. Buckling behavior and axial load transfer assessment of coiled tubing with initial curvature in constant-curvature wellbores. *J. Pet. Sci. Eng.* 195, 107794. <https://doi.org/10.1016/j.petrol.2020.107794>.